Failure Mechanism of Glassy Polymer−Nanoparticle Composites

Jong-Young Lee, Qingling Zhang, Jia-Yu Wang, Todd Emrick, and Alfred J. Crosby*

Department of Polymer Science and Engineering, University of Massachusetts, Amherst, Massachusetts 01003

Received May 9, 2007; Revised Manuscript Received June 15, 2007

ABSTRACT: A model, well-dispersed nanocomposite of surface-modified cadmium selenide (CdSe) nanoparticles (average core diameter of 3.5 nm) blended into polystyrene is prepared such that entropic forces drive the failure mechanism of the nanocomposite. At an optimal volume fraction (∼0.7%) of nanoparticles, the failure strain of the nanocomposite is increased by nearly 60% relative to unfilled polystyrene. The proposed mechanism for this optimal volume fraction is related to the balance of two effects: (1) the decrease in the volume fraction of cross-tie fibrils and (2) the decrease in the extensibility of the craze. These results offer insight into an entropically driven failure of glassy polymer nanocomposites and help guide future design of nanoparticle-based composite materials.

Introduction

The addition of nanoscale fillers to polymer materials has led to markedly enhanced control of a wide range of technically important material properties, from optoelectronic to mechanical.[1,2] For mechanical properties, in particular, nanoscale fillers of different shapes and compositions have led to improvements in processing,[3,4] modulus,[5−8] strain-to-failure,[9,10] and toughness,[8,11−14] relative to microscale fillers. Despite these demonstrated property enhancements, a fundamental rationale describing the origin of such enhanced properties remains elusive for the most basic of nanocomposites. Although it is widely known that the surface-to-volume ratio increases for decreasing nanofiller size, this effect has mostly been considered in the context of enthalpic contributions. As the nanofiller size decreases, entropic contributions to material properties become increasingly important. According to the results from the Balazs, Russell, and Emrick research group, the entropic interaction between particles and polymer chains can lead to nanoparticle patterning in block copolymers[15,16] and material self-healing,[17−19] when particle size is close to the radius gyration of polymer chains. This entropically driven mobility/rearrangement of nanoparticles dispersed in polymer matrix also impacts the failure mechanism of polymer nanocomposites[20] and is the focus of this experimental investigation.

In glassy polymers, crazing is a dominant deformation process, subsequently leading to the formation of cracks and complete fracture of materials. Therefore, understanding the crazing process in the presence of nanoscale fillers is important to define the mechanical robustness of these materials. We previously showed[20] that nanoparticles undergo three stages of rearrangement due to entropic interactions during craze formation and propagation in a polystyrene matrix. These stages are (1) nanoparticle alignment of nanoparticles along the precraze, (2) nanoparticle expulsion of nanoparticles from craze fibrils of the premature craze, and (3) nanoparticle entrapment among craze fibrils in the mature craze. Here, we demonstrate the impact of these nanoparticle-induced processes on craze initiation and growth, breakdown of craze fibrils, and crack propagation.

* To whom correspondence should be addressed: E-mail: crosby@mail.pse.umass.edu, Tel (413) 577-1313, Fax (413) 542-0082.

Cadmium selenide (CdSe) nanoparticles, or quantum dots, of ∼3.5 nm diameter were prepared and functionalized with short polystyrene chains (MW = 1000 g/mol). These PS-functionalized nanoparticles were then blended with polystyrene (MW = 131K g/mol, R_g ∼ 10 nm) to give a dispersion of the nanoparticles in the PS matrix. Through this "grafting to" and blending approach, aggregates of nanoparticle fillers are largely avoided. Importantly, this nanocomposite design precludes the need for other additives (e.g., dispersants) that can alter the crazing process. In addition to aiding nanoparticle dispersion, the effect of both enthalpic interactions and entanglements between the nanoparticles and matrix are minimized by the polystyrene grafts. In this article, we demonstrate that nanoparticles with weak interactions with the surrounding matrix can lead to a significant enhancement of failure properties. This effect is maximized at an optimal volume fraction of nanoparticle fillers due to the balance of two competing mechanisms.

Experimental Section

Synthesis of Surface-Modified Nanoparticles. CdSe nanoparticles were synthesized according to published procedures to give ∼3.5 nm tri-*n*-octylphosphine oxide (TOPO)-covered particles.[21] There TOPO-covered nanoparticles (∼10 mg) were dissolved in anhydrous pyridine and refluxed under argon for 24 h. Most of the remaining pyridine was removed under vacuum, and hexane was added to precipitate the pyridine-covered CdSe nanoparticles. Anhydrous toluene (∼2 mL) and thiol-terminated polystyrene (∼100 mg, MW = 1000, Polymer Source Inc.) were added to the pyridine-covered nanoparticles. This mixture was heated to 60 °C overnight to give a clear solution. Then, hexane was added dropwise until a cloudy suspension was seen. The polystyrene-covered nanoparticles were isolated by centrifugation and purified by repeated dissolution in toluene and precipitation in hexane.

Sample Preparation. The polystyrene-covered CdSe nanoparticles and PS (MW = 131K g/mol, PDI = 1.02, Polymer Source Inc.) were dissolved in toluene at various weight ratios. Using the known densities of CdSe (5.8 g/cm^3)[22] and PS (1 g/cm^3),[23] the nanoparticle volume fraction is calculated.

To quantify the crazing process for polymer nanocomposites, we used a well-established copper grid technique.[24] Sample preparation for this technique began by flow coating a thin film of our polymer−nanoparticle blend on a silicon substrate. The substrate was treated by acetone, toluene, and UV ozone prior to film casting. For flow coating, a volume of 0.1 mL dilute CdSe−PS solution was deposited under the razor blade, and then a moving stage was

10.1021/ma0710479 CCC: $37.00
Published on Web 07/27/2007

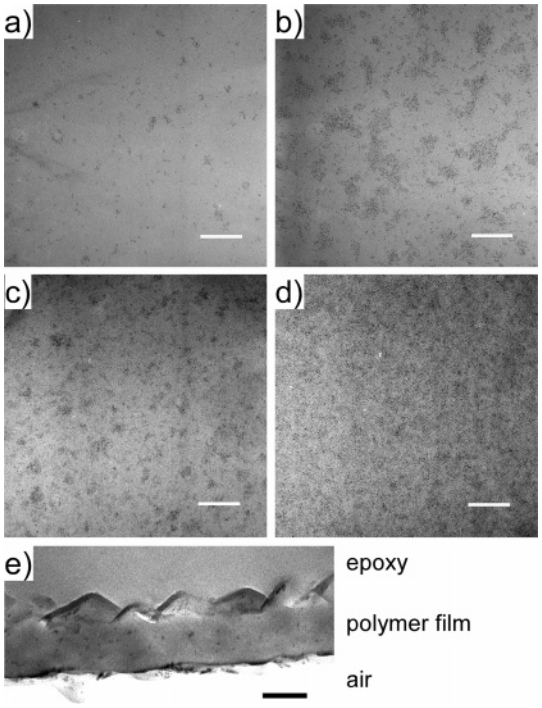

Figure 1. Top-view TEM images of CdSe nanoparticles dispersed in polystyrene matrix with different volume fractions of nanoparticles: (a) 0.14%, (b) 0.34%, (c) 0.68%, and (d) 2.1%; scale bars are 200 nm. (e) Cross-section TEM image of polymer nanocomposite thin film. Volume fraction of nanoparticles is 0.68%; scale bar is 100 nm.

translated at a fixed velocity to create a thin film with uniform thickness (200 ± 20 nm). Within this range, thickness has no effect on craze morphology and crazing process as reported previously.[25−27] Subsequently, we floated the film on water and transferred the film onto a copper grid precoated by PS homopolymer. The film on the copper grid was dried for 12 h and then exposed to toluene vapor to remove wrinkles and increase adhesion between the copper grid and the film. After exposure, the film was dried again for 24 h.

A custom-built, automated strain stage was used to apply fixed strains to the copper grid samples at a strain rate of 2.3×10^{-4} (1/s). One polymer film transferred onto the copper grid sample contains 90 independent grid squares (samples). These samples are all prepared and tested at the same time. Therefore, our results are very consistent and statistical. Polymer nanocomposites with different volume fractions of nanoparticles and PS homopolymer samples were prepared for copper grid testing.

Craze Characterization. To obtain craze growth rate and strains of craze initiation, fibril breakdown, and material failure, the copper grid was unloaded at predefined strains and fixed to a glass slide by tape. We waited 10 min for crazes to reach equilibrium before unloading the copper grid. Subsequently, optical microscopy images were taken for every grid square under bright and dark fields. Dark field enhances the contrast between the craze and the matrix, thus facilitating subsequent image analysis. As developed previously,[27] we used a high-throughput method to collect optical microscopy images and perform subsequent image analysis through a program written in the National Instrument's LabVIEW environment. This image analysis was performed in an objective manner to obtain the number of crazes and area fraction occupied by crazes for each grid square in the whole polymer film.

To characterize the depth and certain morphological aspects of crazes, atomic force microscope (AFM) and transmission electron microscope (TEM) were used. For AFM, the strained copper grid was fixed to a glass slide by tape, and the crazed regions close to the edge of grid bars were scanned to prevent excess deflection.[28] To prepare samples for TEM top-view images, we used a razor blade to cut a grid from the copper grid. This section was then directly mounted into the TEM sample holder. For TEM cross-section image, a thin layer of carbon (~20 nm) was evaporated onto the surface of nanocomposite thin film before samples were embedded in epoxy and cured at 60 °C for overnight. The film was removed from the substrate by dipping into liquid N_2. All samples were microtomed at room temperature with a diamond knife and then transferred to copper grids. TEM measurements were performed on a JEOL TEM200CX at an acceleration voltage of 200 kV.

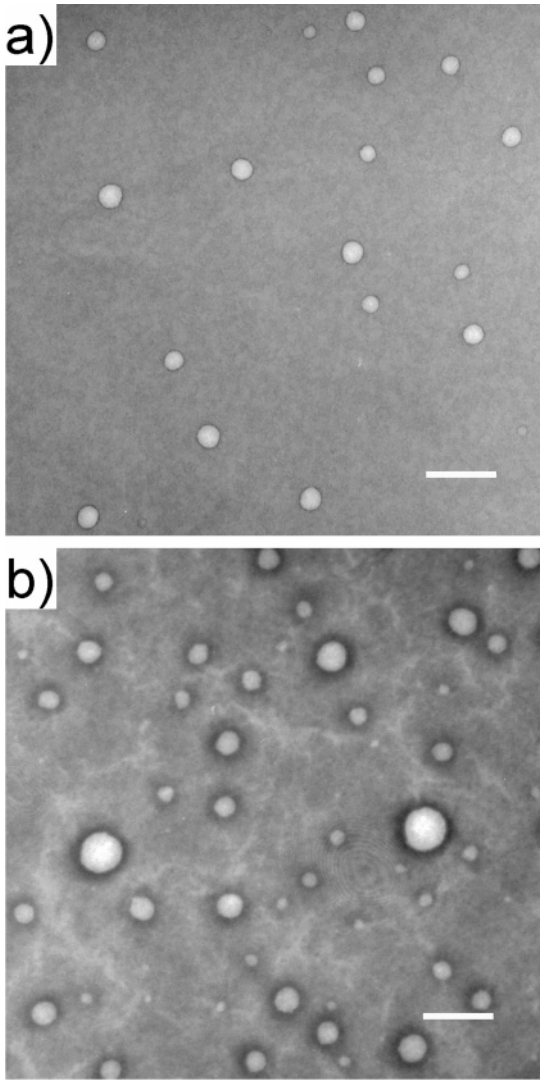

Figure 2. TEM images of holes on nanocomposite thin films with different volume fraction of nanoparticles: (a) 3.3% and (b) 14.5%. Scale bars are 1 μm.

Results and Discussion

Obtaining a uniform dispersion of nanoparticles in polymer matrix is a critically important precursor to the study of mechanical properties of nanocomposites. Based on the controlled synthesis and functionalization of our nanoparticles, uniform size and spatial distribution of particles in PS matrix are found, and individual particles are observed distinctly without aggregation (Figure 1a−d). This uniform dispersion of nanoparticles excludes the effect of aggregation on failure properties of polymer nanocomposites. From the cross-section image of our nanocomposite thin film, the distribution of nanoparticles through the thickness is also observed (Figure 1e).

Uniform dispersion is maintained over all volume fractions tested, but for nanocomposites with volume fraction of nanoparticles (V) ≥3.3%, we observe surface depressions, or holes, on our nanocomposite thin films (Figure 2). These holes form

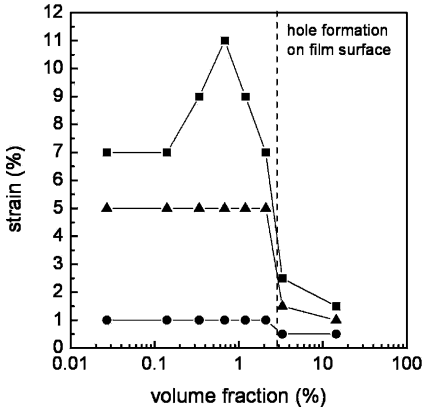

Figure 3. Summary of copper grid test. Strains of craze initiation (circles), fibril breakdown (triangles), and material failure (squares) as a function of volume fraction of nanoparticles. Dotted gray line indicates critical volume fraction above which hole formation on the surface of nanocomposite films is observed.

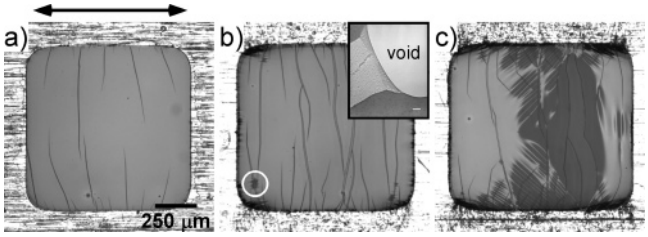

Figure 4. Optical microscope images of polymer films on the copper grid square: (a) Craze initiation. (b) Fibril breakdown (white circle indicates fibril breakdown). Inset: TEM image of a void resulting from fibril breakdown within the craze (scale bar is 500 nm). (c) Failure of materials. Black arrow indicates the direction of tensile force.

spontaneously after the film is cast on the silicon substrate. Since these "surface defects" also contribute to the failure of polymer thin films, our discussion will be divided into two sections according to nanocomposites with low ($V < 3.3\%$) and high ($V \geq 3.3\%$) volume fraction of nanoparticles.

Low Volume Fraction Nanocomposites ($V < 3.3\%$). According to classic crazing models, the crazing process includes four stages based on the sequence of material failure: craze initiation, craze growth, fibril breakdown, and crack propagation. We discuss how nanoparticles impact these four stages.

a. Craze Initiation. Crazes are narrow (100 nm−2 μm) and long (50−1000 μm) regions of dense arrays of fibrils (diameter is 5−30 nm) of glassy polymers. They are nucleated from surface defects or inclusions. According to accepted theories,[29] these regions lead to stress concentration and the existence of a hydrostatic stress, which causes local yielding, cavitation, growth of voids, and subsequent formation of craze nuclei. In our measurements, craze initiation strain is defined as the strain at which over 50% of grids is observed with crazes. For samples with $V < 3.3\%$, craze initiation occurs statistically at 1% strain, which is the same as PS homopolymer (Figure 2a). According to this result, the existence of nanoparticles in PS matrix does not lead to a significant change in the local stress field to alter craze initiation strain at low V. Larger defects associated with the edges of the copper grid cause most crazes to initiate from this location (Figure 4a).

b. Craze Growth. Crazes grow in length by a meniscus instability and in thickness by drawing polymer chains from the unyielded matrix into the craze (surface drawing).[29] As strain increases, crazes become wider and longer. To follow the sequence of craze growth, we divide a craze into three regions: precraze, premature craze, and mature craze. The precraze is a locally yielded region at the leading tip of the craze. Following

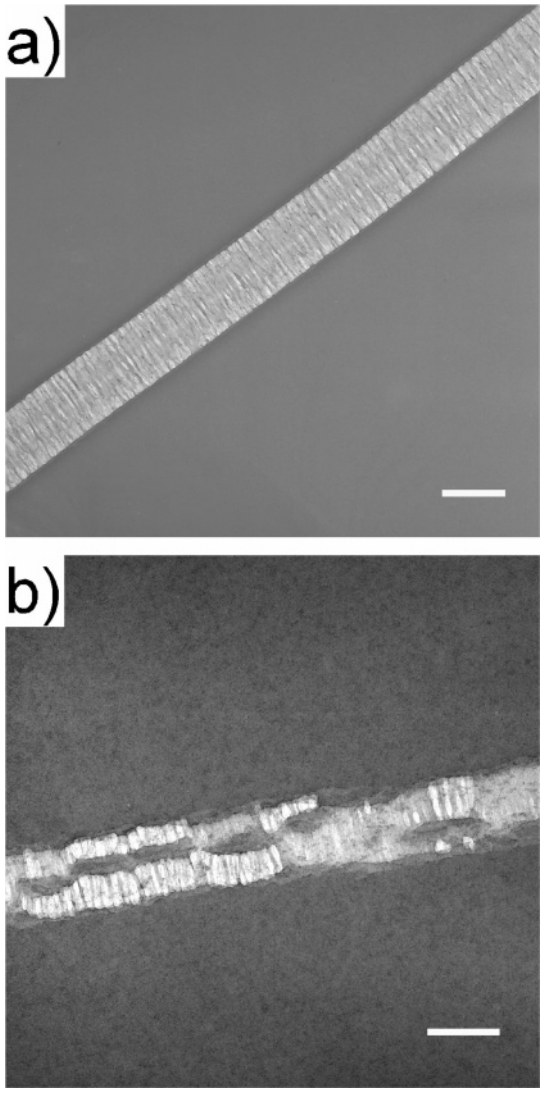

Figure 5. TEM images of premature crazes in (a) polystyrene homopolymer and (b) nanocomposite (volume fraction of nanoparticles is 2.1%). Scale bars are 400 nm.

the precraze, nanofibrils form in the premature craze and eventually lead to the formation of the mature craze with nanofibril arrays at a larger volume fraction.[24,29] In our nanocomposites with $V < 0.68\%$, the premature craze is an integral craze, similar to a craze in PS homopolymer (Figure 5a). However, for samples with $V \geq 0.68\%$, the premature craze consists of multiple "secondary crazes" (Figure 5b). This morphological change was reported in a previous publication.[20]

Craze growth is an energetic process where the applied strain energy drives the formation of craze fibrils and growth of crazes (advancing and widening). Using a craze growth rate, we can compare the energetics of growing crazes in the different nanoparticle volume fraction materials. The craze growth rate (R_c) is defined as the increase of normalized area fraction (A_f) per unit strain (ϵ).[27]

$$R_c = \frac{\partial A_f}{\partial \epsilon}$$

$$A_f = \frac{\text{area fraction occupied by crazes per grid}}{\text{number of crazes per grid}} \times 100$$

A_f is equivalent to the average area fraction of one craze in one grid square. Although A_f is linked to both craze nucleation (proportional to the number of crazes) and craze growth, the

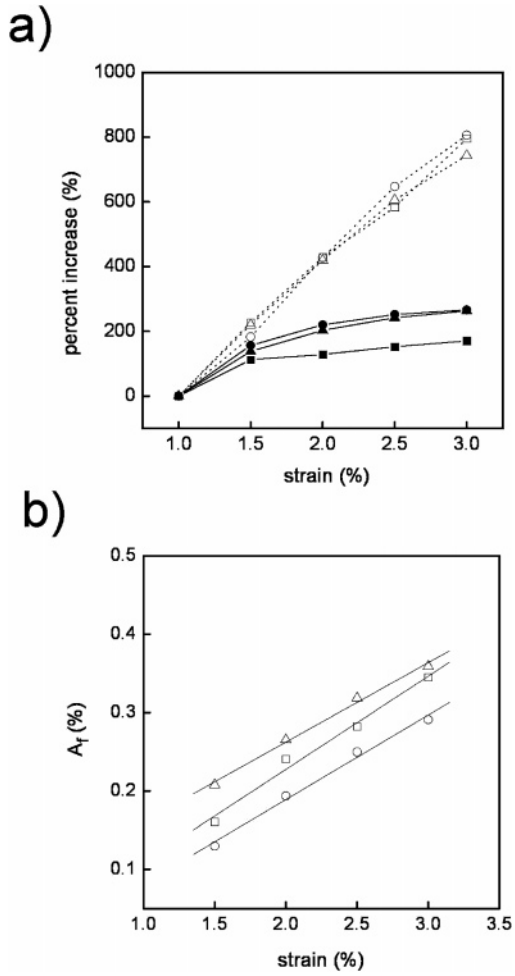

Figure 6. (a) Percent increase of the number of crazes (solid line) and area fraction of crazes (dotted line) per grid and (b) plot of normalized area fraction (A_f) as a function of tensile strain for nanocomposites with different volume fraction of nanoparticles: 0% (square), 0.68% (circle), and 2.1% (triangle). Gray straight lines in (b) are obtained from linear fitting.

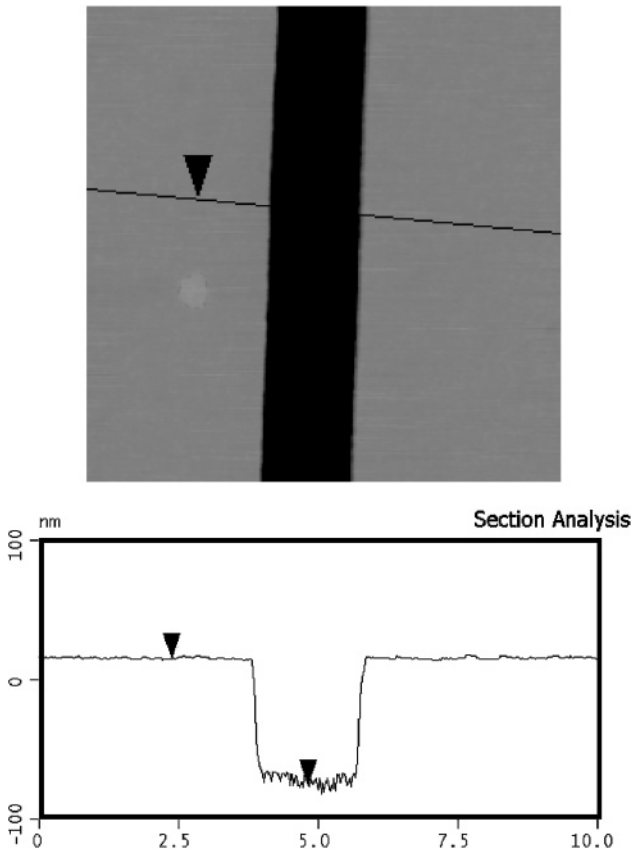

Figure 7. AFM image and section profile of the craze in polymer nanocomposite (volume fraction of nanoparticles is 0.68%). The image size is 10 μm × 10 μm. Film thickness is 237 nm; depth of the craze is 90 nm.

percent increase of the number of crazes plateaus after 1.5% strain, while A_f continues to increase as a function of applied strain (Figure 6a). Therefore, A_f is dominated by craze growth, not nucleation, after 1.5% strain. By plotting A_f as a function of strain after 1.5% strain (Figure 6b), the relationship between A_f and strain is linear and the slope is the craze growth rate.[27] For clarity, only three volume fractions are plotted in Figure 6. Other samples have similar trend as ones shown in Figure 6. The applied strain energy for craze growth is inversely proportional to the slope (R_c).[27] Materials with $V < 3.3\%$ have the same craze growth rate, as indicated in Figure 6b. Thus, the formation of secondary crazes and rearrangement of nanoparticles during crazing do not alter the craze growth rate. Consequently, the energetics of craze growth in our nanocomposites is similar to PS homopolymer.

In addition to growing in length and width, crazes in thin films also experience a micronecking process in the thickness direction (Figure 7). One quantity that describes this micronecking is the ratio of craze depth to total film thickness.[30] Micronecking requires the extension of craze fibrils from the uncrazed surface to the surface depth of craze section. Therefore, the depth-to-thickness ratio is related to fibril extension ratio of crazes[31] and consequently stability or breakdown of craze fibrils. In our measurements, all crazes in nanocomposites have the same depth-to-thickness ratios of 0.38 ± 0.005, which is close to 0.37 of PS homopolymer.[27,28] This result suggests that nanoparticles do not affect the micronecking process and the associated fibril extension ratio.

c. Breakdown of Craze Fibrils. During the craze widening process, the eventual breakdown of craze fibrils occurs at the craze−bulk interface by chain scission or disentanglement.[32,33] Fibril breakdown results in the formation of microvoids within the craze (Figure 4b, inset), which eventually grow into a crack (crack initiation) and lead to the failure of materials. In the copper grid experiments, fibril breakdown is observed as local wrinkles within the craze under an optical microscope (Figure 4b), and fibril breakdown strain is defined as over 50% of the grids observed with local wrinkles. One term to describe fibril breakdown is "fibril stability",[32] defined as the difference between fibril breakdown strain and craze initiation strain. According to classic crazing model, fibril stability is related to the fibril extension ratio and craze growth. For fibril extension ratio, large fibril extension ratio facilitates fibril breakdown, resulting in lower fibril stability.[33] For craze growth, the probability of fibril breakdown decreases with craze growth rate (R_c) decreasing, consequently leading to higher fibril stability. As mentioned early, crazes in samples with $V < 3.3\%$ have the same fibril extension ratio and craze growth rate. Therefore, they have the same fibril stability. The same fibril stability and craze initiation strain among these samples give rise to the independence of fibril breakdown strain of V (Figure 3).

d. Crack Propagation. In addition to fibril breakdown (crack initiation), the growth of the void or crack resulting from fibril breakdown plays an important role in the material's failure. The failure strain is defined as the strain at which over 50% of the grid have macroscopic failure (Figure 4c). Since nanoparticles have no effect on fibril breakdown, the impact of nanoparticles

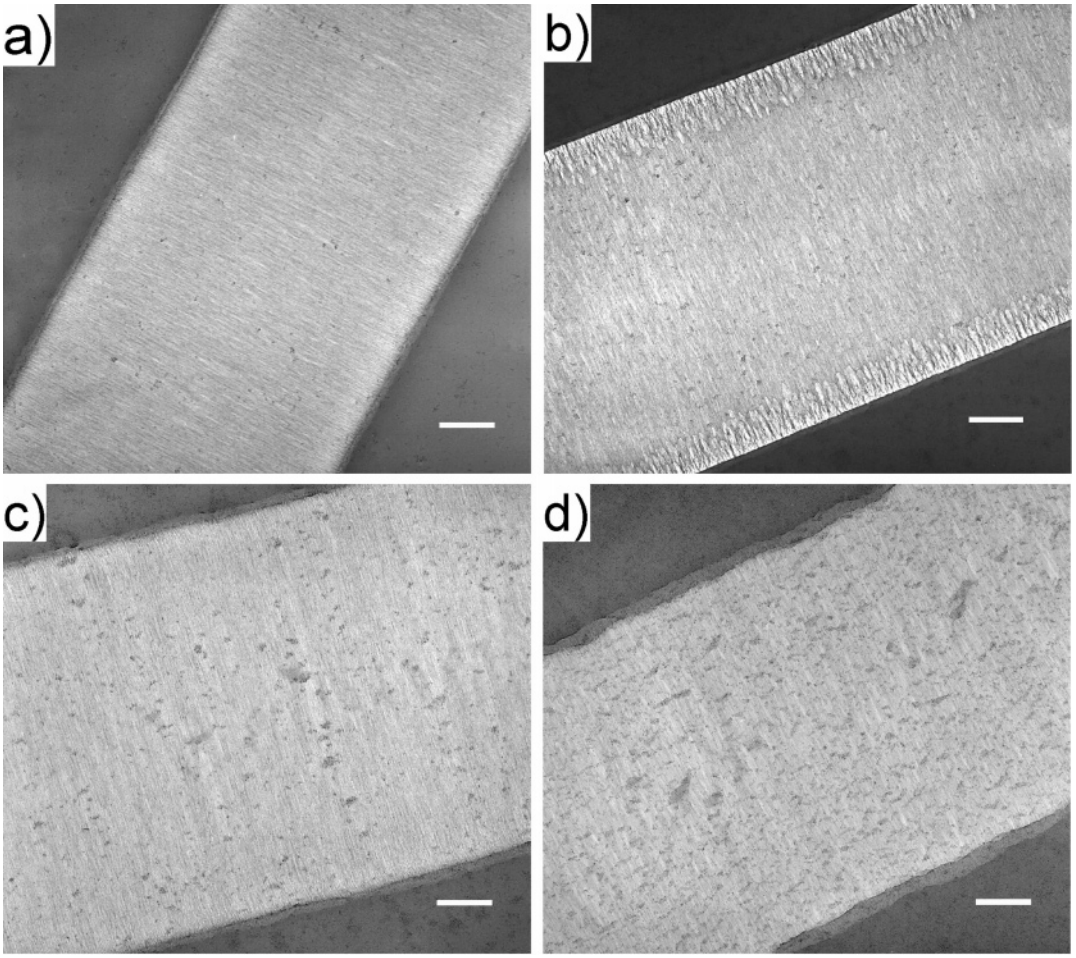

Figure 8. TEM images of mature crazes in nanocomposites with different volume fractions of nanoparticles: (a) 0.14%, (b) 0.34%, (c) 0.68%, and (d) 2.1%. Scale bars are 300 nm.

on the failure strain of nanocomposites is attributed to the propagation of the crack through the craze. In Figure 3, a maximum failure strain at an optimal V is found. This maximum failure strain suggests a balance between two competing mechanisms: one that leads to an increase in failure strain as a function of V and one that leads to a decrease in failure strain as a function of V.

One possible explanation for increasing the failure strain with increasing V is that the nanoparticles are serving as plasticizers (due to the existence of low-MW polystyrene ligands), which decrease the elastic modulus and increase the density of chain entanglements within craze fibrils.[34] The decrease in elastic modulus alters the strain energy applied to the material as a function of strain; therefore, an increased craze initiation strain and strain-to-failure is typically observed for plasticizers that decrease the composite modulus.[34] Although we measure a decreased modulus as a function of V,[35] the craze initiation strain is independent of V in our materials. Therefore, the decrease in elastic modulus is not a main mechanism for the enhanced ductility of these nanocomposites. The existence of plasticizers also can lead to the increase in the density of chain entanglement within craze fibrils, consequently leading to an increase in failure strain. This effect causes a change in the fibril extension ratio. However, the fibril extension ratio of our nanocomposites is independent of V. Consequently, the increase in failure stain of our nanocomposites as a function of V is not consistent with the nanoparticles serving as a plasticizer.

An alternative mechanism, which is consistent with our observations, for the increased failure strain as a function of V is related to the cross-tie fibrils within the craze structure. As reported previously, during craze widening, an entangled strand spanning two fibrils in the craze−bulk interface must be segmented and then drawn into two fibrils.[29] Occasionally, the piling up of several entangled strands at the craze−bulk interface occurs. This pile of strands is difficult to break energetically compared to a single strand. Thus, the craze−bulk interface bypasses these strands. This process leads to the formation of cross-tie fibrils, which connect two main fibrils within the caze.[36] According to the model of Brown and Kramer et al.,[37,38] cross-tie fibrils lead to lateral load transfer between main fibrils. This load transfer causes stress concentration in the center of the main fibril closest to a crack tip within the craze and facilitates breakdown of main fibrils to grow the microvoid or crack. By considering the craze as an anisotropically elastic strip, the fracture toughness (G_c) is related to the ratio of tensile modulus parallel to main fibrils (E_{22}) to the modulus perpendicular to main fibrils (E_{12}), and the relative volume fraction of main fibrils (f_m) to cross-tie fibrils (f_c):[37,38]

$$G_c \propto \left(\frac{E_{22}}{E_{12}}\right)^{1/2} \propto \left(\frac{f_m}{f_c}\right)^{1/2}$$

As mentioned in our previous paper,[20] nanoparticles are entrapped within the mature craze during craze widening and are surrounded by craze fibrils. These entrapped nanoparticles disrupt the formation of cross-tie fibrils. As V increases, more nanoparticles are entrapped in the craze in our nanocomposites (Figure 8), implying more nanoparticles passing through craze−

bulk interface with V increasing. Because of the increased mobility of polymer segments at an enthalpically neutral nanoparticle surface, nanoparticles in the craze−bulk interface can serve as a separator between polymer chains. Therefore, the probability for chains to form pile-up entangled strands at the craze−bulk interface decreases as V increases. Consequently, less cross-tie fibrils form in the craze as V increases. Therefore, f_c decreases and greater strain is required to exceed G_c for crack propagation according to eq 1. This effect contributes to an increase in failure strain as a function of V (Figure 2b).

In a competing manner, the entrapped nanoparticles within the craze also affect the extension properties of the craze. Similar to treatments by Brown, Hui, and Kramer,[37,38] the crazed region can be considered as an elastic strip with a constant stress on the boundary between the craze and unyielded polymer.[37,38] Because of the entrapment of nanoparticles within the craze, the crazed region can be considered as a "polymer composite". According to Nielsen's model for polymer composites,[39] the macroscopic failure strain of composites decreases due to the decrease in the volume fraction of compliant material, i.e., polymer matrix, as the volume fraction of rigid particle filler increases. Consequently, according to a simple geometric derivation, the strain-to-failure (ϵ_B) of a polymer composite with good filler−matrix adhesion can be related to the volume fraction (ϕ) of fillers by[39]

$$\epsilon_B \sim 1 - \phi^{1/3}$$

If poor filler−matrix adhesion is assumed, ϵ_B decreases as a function of ϕ with a smaller decaying rate.[39] In either case, an increased particle volume fraction leads to a decreased ϵ_B. In our materials, more nanoparticles are entrapped within the crazes as V increases (Figure 8); therefore, the extensibility of the craze decreases with V increasing. Combining these two processes, the, failure strain of our nanocomposites reaches a maximum at an optimal volume fraction with V increasing (Figure 3).

High Volume Fraction Nanocomposites ($V \geq 3.3\%$). As mentioned above, surface depressions form spontaneously on the nanocomposite thin films when the loading percentage of nanoparticles exceeds 3.3 vol %. The density of surface depressions increases as V increases (Figure 2), but their depth (50 nm from AFM) and lateral dimensions ($\sim$0.5 μm) are independent of V. Although the mechanism for the formation of these depressions is currently unexplained, the existence of these "surface defects" can alter the local stress field and the local crazing process. These holes are sudden changes in the local film thickness. Specifically, a large stress concentration is generated at the boundaries of holes, similar to dust particles that are responsible for early fibril breakdown and material failure.[32] In the nanoparticle composites discussed here, more "surface defects" are found in the sample with $V = 14.7\%$ compared to $V = 3.3\%$ (Figure 2). Accordingly, fibril breakdown and material failure occurs at lower strain for $V = 14.7\%$ compared to the sample with $V = 3.3\%$ (Figure 3). This result is similar to findings in previous research,[27] where hole formation on block copolymer thin films leads to early failure of materials. In both cases, the depth of the depressions is $\sim$50 nm, the lateral dimension is on the order of 1 μm, and the thickness of the film is 135−245 nm.

Although the failure strain trend is similar to block copolymer films, the initiation strain decreases at higher V for the nanoparticle composites. These results are not consistent with hole structures on model block copolymer films (i.e., hole structures leads to the increase in craze initiation strain).[27] This inconsistency suggests an important contribution from the presence of the nanoparticles, but further exploration remains for a future investigation.

Conclusion

For nanocomposites with volume fraction of nanoparticles $<3.3\%$, nanoparticles have no effect on craze initiation, craze growth, and fibril extension ratio. However, we find that nanoparticles impact crack propagation, leading to an increase in failure strain by 60% at an optimal volume fraction of $\sim$0.7%. This optimal volume fraction represents the balance of two mechanisms: (1) increasing fracture toughness (G_c) with decreasing number of cross-tie fibrils and (2) decreasing extensibility of the craze with increased volume fraction of nanoparticles entrapped within the craze. These results offer insight into the impact of nanoparticles on the crazing process and failure of glassy polymer nanocomposites based on entropic interactions and help to predict the effective design of nanoparticle-based materials.

Acknowledgment. Funding for this project is provided by the NSF-MRSEC at the University of Massachusetts, Petroleum Research Fund of the American Chemical Society, and the Department of Energy (DE-FG-02-96ER45).

References and Notes

(1) Sanchez, C.; Julian, B.; Belleville, P.; Popall, M. *J. Mater. Chem.* **2005**, *15*, 3559−3592.
(2) Thostenson, E. T.; Li, C. Y.; Chou, T. W. *Compos. Sci. Technol.* **2005**, *65*, 491−516.
(3) Zhang, Q.; Archer, L. A. *Langmuir* **2002**, *18*, 10435−10442.
(4) Sternstein, S. S.; Zhu, A. J. *Macromolecules* **2002**, *35*, 7262−7273.
(5) Sumita, M.; Tsukihi, H.; Miyasaka, K.; Ishikawa, K. *J. Appl. Polym. Sci.* **1984**, *29*, 1523−1530.
(6) Vollenberg, P. H. T.; Heikens, D. *Polymer* **1989**, *30*, 1656−1662.
(7) Kojima, Y.; Usuki, A.; Kawasumi, M.; Okada, A.; Fukushima, Y.; Kurauchi, T.; Kamigaito, O. *J. Mater. Res.* **1993**, *8*, 1185−1189.
(8) Wu, C. L.; Zhang, M. Q.; Rong, M. Z.; Friedrich, K. *Compos. Sci. Technol.* **2002**, *62*, 1327−1340.
(9) Ash, B. J.; Siegel, R. W.; Schadler, L. S. *Macromolecules* **2004**, *37*, 1358−1369.
(10) Hsiao, C. C.; Lin, T. S.; Cheng, L. Y.; Ma, C. C. M.; Yang, A. C. M. *Macromolecules* **2005**, *38*, 4811−4818.
(11) Ou, Y. C.; Yang, F.; Yu, Z. Z. *J. Polym. Sci., Part B* **1998**, *36*, 789−795.
(12) Wilbrink, M. W. L.; Argon, A. S.; Cohen, R. E.; Weinberg, M. *Polymer* **2001**, *42*, 10155−10180.
(13) Thio, Y. S.; Argon, A. S.; Cohen, R. E.; Weinberg, M. *Polymer* **2002**, *43*, 3661−3674.
(14) Chan, C. M.; Wu, J. S.; Li, J. X.; Cheung, Y. K. *Polymer* **2002**, *43*, 2981−2992.
(15) Thompson, R. B.; Ginzburg, V. V.; Matsen, M. W.; Balazs, A. C. *Science* **2001**, *292*, 2469−2472.
(16) Lee, J. Y.; Thompson, R. B.; Jasnow, D.; Balazs, A. C. *Phys. Rev. Lett.* **2002**, 89.
(17) Tyagi, S.; Lee, J. Y.; Buxton, G. A.; Balazs, A. C. *Macromolecules* **2004**, *37*, 9160−9168.
(18) Lee, J. Y.; Buxton, G. A.; Balazs, A. C. *J. Chem. Phys.* **2004**, *121*, 5531−5540.
(19) Gupta, S.; Zhang, Q. L.; Emrick, T.; Balazs, A. C.; Russell, T. P. *Nat. Mater.* **2006**, *5*, 229−233.
(20) Lee, J.-Y.; Zhang, Q.; Emrick, T.; Crosby, A. J. *Macromolecules* **2006**, *39*, 7392.
(21) Peng, Z. A.; Peng, X. G. *J. Am. Chem. Soc.* **2001**, *123*, 183−184.
(22) *Handbook of Chemistry and Physics*, 77th ed.; Lide, D. R., Ed.; CRC Press: Boca Raton, FL, 1996−1997.
(23) Fox, T. G.; Flory, P. J. *J. Polym. Sci.* **1954**, *14*, 315−319.
(24) Lauterwasser, B. D.; Kramer, E. J. *Philos. Mag. A* **1979**, *39*, 469−495.
(25) Donald, A. M.; Chan, T.; Kramer, E. J. *J. Mater. Sci.* **1981**, *16*, 669−675.
(26) Chan, T.; Donald, A. M.; Kramer, E. J. *J. Mater. Sci.* **1981**, *16*, 676−686.
(27) Lee, J.-Y.; Crosby, A. J. *Macromolecules* **2005**, *38*, 9711−9717.
(28) Crosby, A. J.; Fasolka, M. J.; Beers, K. L. *Macromolecules* **2004**, *37*, 9968−9974.

(29) Kramer, E. J. *Adv. Polym. Sci.* **1983**, *52*−*3*, 1−56.
(30) Yang, A. C. M.; Kunz, M. S.; Logan, J. A. *Macromolecules* **1993**, *26*, 1767−1773.
(31) Lin, J. H.; Yang, A. C. M. *Macromolecules* **2001**, *34*, 3698−3705.
(32) Yang, A. C. M.; Kramer, E. J.; Kuo, C. C.; Phoenix, S. L. *Macromolecules* **1986**, *19*, 2010−2019.
(33) Kramer, E. J.; Berger, L. L. *Adv. Polym. Sci.* **1990**, *91/91*, 2−68.
(34) Yang, A. C. M.; Kramer, E. J.; Kuo, C. C.; Phoenix, S. L. *Macromolecules* **1986**, *19*, 2020−2027.
(35) Lee, J.-Y.; Su, K. E.; Chan, E. P.; Zhang, Q.; Emrick, T. Manuscript in preparation.
(36) Miller, P.; Buckley, D. J.; Kramer, E. J. *J. Mater. Sci.* **1991**, *26*, 4445−4454.
(37) Brown, H. R. *Macromolecules* **1991**, *24*, 2752−2756.
(38) Hui, C. Y.; Ruina, A.; Creton, C.; Kramer, E. J. *Macromolecules* **1992**, *25*, 3948−3955.
(39) Nielsen, L. E. *J. Appl. Polym. Sci.* **1966**, *10*, 97.

MA0710479